ARTICLE

Research on VSG Frequency Characteristics and Energy Storage Device Capacity and Charge-Discharge Characteristics Based on Feedforward Branch

Baoge Zhang[1], Shanyan Ping[1,*], Haoliang Shi[2], Yi Long[1], Boxiang Wu[1] and Yuemin Jiao[1]

[1]School of Automation & Electrical Engineering, Lanzhou Jiaotong University, Lanzhou, China

[2]Qinghai Nationalities University, Xining, China

[*]Corresponding Author: Shanyan Ping. Email: pingshanyan@foxmail.com

ABSTRACT

Renewable energy is connected to the grid through the inverter, which in turn reduces the inertia and stability of the power grid itself. The traditional grid-connected inverter does not have the function of voltage regulation and frequency regulation and can therefore no longer adapt to the new development. The virtual synchronous generator (VSG) has the function of voltage regulation and frequency regulation, which has more prominent advantages than traditional inverters. Based on the principle of VSG, the relationship between the frequency characteristics and the energy storage capacity of the feedforward branch-based virtual synchronous machine (FVSG) is derived when the input power and grid frequency change. Reveal the relationship between the virtual inertia coefficient, damping coefficient, and frequency characteristics of VSG and energy storage capacity. An energy storage configuration method that meets the requirements of frequency variation characteristics is proposed. A mathematical model is established, and the Matlab/Simulink simulation software is used for modeling. The simulation results verify the relationship between the inertia coefficient, damping coefficient, and energy storage demand of the FVSG.

Nomenclature

T_s	Mechanical torque
T_e	Electromagnetic torque
D	Damping coefficient
J	Moment of inertia
P_{in}	Input power
P_{out}	Output power
P_{in0}	Rated input power
P_{out0}	Rated output power
P_{es}	The charging and discharging power of the energy storage device
ω	Mechanical angular frequency
ω_0	Rated angular frequency

ω_g	Grid frequency
$\Delta\omega$	Difference between output corner frequency and rated corner frequency
ΔP_{in}	Difference between actual input power and rated input power
ΔP_{out}	Difference between actual output power and rated output power
u_a, u_b, u_c	Output three-phase voltage
u_{ga}, u_{gb}, u_{gc}	Three-phase voltage of the grid
U_{dc}	DC bus voltage
U	Valid values for u_a, u_b and u_c
U_g	Valid values for u_{ga}, u_{ga} and u_{gc}
U_0	Ratings for u_a, u_b and u_c
δ_0	Rated power angle
H	Feedforward gain
Ees	Charge and discharge energy of energy storage device
K	Synchronization factor

1 Introduction

With the rapid development and innovation of what is often called "new energy," represented by photovoltaic and wind power, these resources have been more widely used and worked into power grids over recent years [1–3]. However, due to the constraints of output characteristics, new energy power sources are generally connected to the grid through power electronic interface devices. Therefore, this new energy type is classified as inverter-based power [4,5]. At present, these new energy sources are mainly connected to the grid through inverters because inverters do not have the inertia and damping characteristics of generators, and virtual synchronous generators (VSG) can simulate the inertia and damping inertia of synchronous generators, once VSG was proposed, it was widely studied and applied [6,7]. VSG has no rotor and mainly simulates the moment of inertia and damping generated by the rotor through control algorithms. The VSG realizes grid connection by affecting the generator's actual output characteristics so that the grid's stability is consistent with the traditional generator, which is beneficial to the operation and management of the grid. Inertia and damping are mainly determined by the control algorithm of the inverter and the parameters of the energy storage device. There are many kinds of research on the control algorithm and stability of the VSG, and less research on the relationship between the VSG parameters and the energy storage devices [8–10].

Geng et al. [11] summarized the principal models of various VSGs. Zhang et al. [12] proposed a power quality control strategy based on a small-signal virtual synchronous machine microgrid. Chen et al. [13] proposed an improved control strategy for the converter at the receiving end of the VSG. Daili et al. [14] proposed a VSG frequency control strategy based on digital frequency protection to improve frequency stability and maintain the dynamic safety of inertial systems. Yan et al. [15] proposed an inertial fuzzy control that allows dynamic adjustment of inertia. Yan et al. [16] operated the PV system at sub-optimal operating points and performs a support strategy that simulates inertia and primary FM characteristics. Gao et al. [17] combined PV and energy storage to achieve both virtual inertia and independent operation. Lu et al. [18–23] analyzed the improved VSG control algorithm and its implementation; Song et al. [24–26] analyzed the strategy of virtual inertia allocation and regulation of multi-VSG systems. The parameters of the VSG require not only the setting of the control algorithm but also the support of the energy storage capacity. Most of the aforementioned previous literature does not examine the impact of energy storage. Xing et al. [27] studied the energy storage configuration methods on different occasions to find the optimal energy storage configuration scheme. Still, it did not explain the energy storage requirements in terms of inertia and damping.

Meng et al. [28] have studied the energy storage model and the power control method of charging and discharging for the photovoltaic application of VSG but have not deduced the capacity requirements of VSG inertia and damping and energy storage. The Gao et al. [17] studied the optimal configuration structure of the energy storage system. Still, it has not yet calculated the relationship between the inertia and damping of the VSG and the capacity of the energy storage device.

This paper first proposes a feed-forward branch-based virtual synchronous generator (FVSG) system for the optimisation of the robustness of conventional VSGs. The relationship between the frequency characteristics and parameters of the FVSG, the inertia and damping coefficients, and the capacity and charging/discharging characteristics of the energy storage unit are then all analysed in the presence of input power disturbances and grid frequency variations. The corresponding relationships are derived to give the optimal configuration parameters of the energy storage unit. The results of the study can be used for the design of FVSG parameters and the capacity configuration of energy storage devices.

2 Establishment of FVSG Mathematical Model

2.1 Mathematical Model of Traditional VSG

The synchronous generator has a rotor and has a particular inertia, so the system's frequency will not change abruptly in a short time. The VSG introduces virtual inertia moment control in the control algorithm of the inverter to simulate the rotor inertia of the synchronous generator. The mechanical rotation equation of the synchronous generator is shown in equation [27,29,30]

$$J\frac{d\omega}{dt} = T_s - T_e - D(\omega - \omega_0)$$

where, T_s is the mechanical torque input by the generator; T_e is the electromagnetic torque of the generator; D is the damping coefficient of the generator; J is the moment of inertia of the generator; ω is the mechanical angular frequency of the rotor; ω_0 is the rated angle of the rotor frequency.

The mechanical power of the synchronous generator is defined as equation

$$P_s = T_s \cdot \omega_0$$

The electromagnetic power of the synchronous generator is defined as equation

$$P_e = T_e \cdot \omega_0$$

The equation can be obtained from equation to

$$J\frac{d\omega}{dt} = \frac{P_s}{\omega_0} - \frac{P_e}{\omega_0} - D(\omega - \omega_0)$$

The VSG simulates the rotor motion equation of the synchronous generator mainly by controlling the control algorithm of the inverter. It can simulate the moment of inertia and damping characteristics of the synchronous generator and realize the stability and droop characteristics of the output voltage and frequency of the virtual synchronous generator. The schematic diagram of the virtual synchronization machine is shown in Fig. 1.
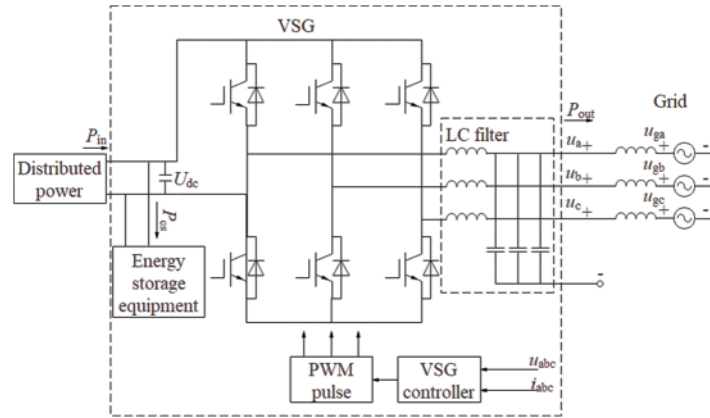
Figure 1: Diagram of VSG system

In the figure: P_{out} is the output power; P_{in} is the input power; P_{es} is the charging and discharging power of the energy storage device; u_a, u_b and u_c are the output three-phase phase voltages; u_{ga}, u_{gb}, and u_{gc} are the three-phase phase voltages of the grid; U_{dc} is the input DC bus voltage.

When the number of pole pairs of the VSG is considered to be 1, the angular frequency of the induced electromotive force is the same as the mechanical angular frequency of the rotor rotating, and the equation can be obtained from the equation

$$P_{in} - P_{out} = J\omega_0 \frac{d\omega}{dt} + D\omega_0(\omega - \omega_0)$$

where, J is the moment of inertia of the VSG; D is the damping coefficient of the VSG.

Use P_{in0} to represent the rated input power of the VSG, and P_{out0} to represent the rated output power of the VSG.

Let $\Delta\omega = \omega - \omega_0$, $\Delta P_{in} = P_{in} - P_{in0}$, $\Delta P_{out} = P_{out} - P_{out0}$; then $\Delta\omega$ represents the difference between the output angular frequency of the VSG and the rated angular frequency. ΔP_{in} means the difference between the actual input power of the VSG and the rated input power. ΔP_{out} represents the difference between the real output power and the rated output power of the VSG, so the equation can be obtained from the equation

$$P_{in0} + \Delta P_{in} - P_{out0} - \Delta P_{out0} = J\omega_0 \frac{d(\omega_0 + \Delta\omega)}{dt} + D\omega_0\Delta\omega$$

Equations can be obtained when the VSG operates under the rated steady-state operating conditions.

$$\omega = \omega_0$$

$$P_{in0} = P_{out0}$$

Equation can be obtained from equations to

$$\Delta P_{in} - \Delta P_{out} = J\omega_0 \frac{d\Delta\omega}{dt} + D\omega_0\Delta\omega$$

The active output power of the generator can be expressed as equation

$$P_{\text{out}} = 3\frac{UU_{\text{g}}}{\omega L}\sin\delta$$

where, U represents the effective value of u_{a}, u_{b} and u_{c}; U_{g} represents the effective value of u_{ga}, u_{gb} and u_{gc}. Let $\Delta U = U - U_0$, $\Delta\delta = \delta - \delta_0$; U_0 represents the rated of value of u_{a}, u_{b} and u_{c}; δ_0 represents the rated power angle of VSG. Without considering the changes in VSG output voltage and grid voltage, equation can be obtained

$$P_{\text{out0}} + \Delta P_{\text{out}} = 3\frac{UU_{\text{g}}}{\omega L}\sin(\delta_0 + \Delta\delta)$$

Since $\Delta\delta$ is smaller, there are $\cos\Delta\delta \approx 1$, $\sin\Delta\delta \approx \Delta\delta$, $\omega_0 + \Delta\omega \approx \omega_0$. So the equation can be obtained

$$P_{\text{out0}} + \Delta P_{\text{out}} = 3\frac{UU_{\text{g}}}{\omega_0 L}\sin\delta_0 + 3\frac{UU_{\text{g}}}{\omega_0 L}\cos\delta_0\Delta\delta$$

When U and U_{g} are constant, because of $P_{\text{out0}} = 3\frac{U_0 U_{\text{g}}}{\omega_0 L}\sin\delta_0$, the equation can be obtained

$$\Delta P_{\text{out}} = 3\frac{U_0 U_{\text{g}}}{\omega_0 L}\cos\delta_0\Delta\delta$$

Let $K = 3\frac{U_0 U_{\text{g}}}{\omega_0 L}\cos\delta_0$, is the synchronization coefficient of VSG. Then equation can be expressed as equation

$$\Delta P_{\text{out}} = K\Delta\delta$$

The variation of the VSG angle of attack can be expressed as equation

$$\Delta\delta = \int_0^t (\Delta\omega - \Delta\omega_{\text{g}})\mathrm{dt}$$

where, $\Delta\omega_{\text{g}} = \omega_{\text{g}} - \omega_0$, ω_{g} is the grid frequency.

Equations are the small-signal time-domain mathematical models of the VSG. Laplace transform can be used to obtain the small-signal frequency-domain mathematical model of VSG, as shown in equations to

$$\Delta P_{\text{in}} - \Delta P_{\text{out}} = J\omega_0\Delta\omega s + D\omega_0\Delta\omega$$

$$\Delta P_{\text{out}} = K\Delta\delta$$

$$\Delta\delta = \frac{\Delta\omega - \Delta\omega_{\text{g}}}{s}$$

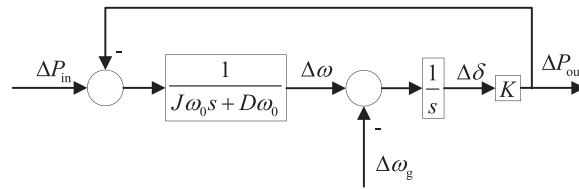According to equations to, the transfer function block diagram of VSG can be obtained as shown in Fig. 2.

Figure 2: Small signal model of VSG

2.2 FVSG Mathematical Model

A robust optimal control method of FVSG is proposed. In the case of input power and grid frequency disturbance, the VSG can maintain relative stability, and the transient process is smooth without oscillation. After the feedforward branch is added to the controller of the VSG, the control block diagram is shown in Fig. 3.
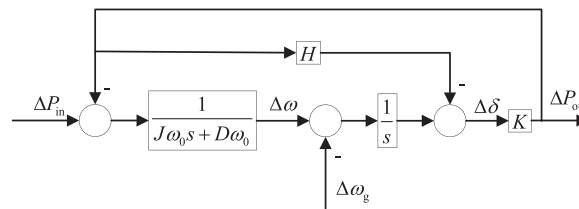

Figure 3: Small signal model of FVSG

In the figure, H is the feedforward gain, and the designed feedforward branch gain H is shown in the equation

$$H = \frac{1}{\omega_0 D}$$

The increased feedforward gain does not affect the power linearization process. Therefore, the FVSG and the traditional VSG have the same synchronization coefficient K. After performing an equivalent transformation on the small-signal model in Fig. 3, the small-signal model is shown in Fig. 4 can be obtained.
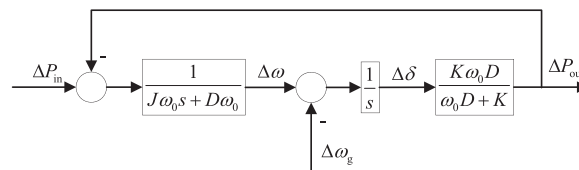

Figure 4: Equivalent transformed FVSG small-signal model

The inertial and frequency modulation responses of FVSG are shown in Fig. 5. During the entire frequency response process, the system's rate-of-change amplitude, peak frequency, adjustment time, and steady-state frequency appear in sequence in time.
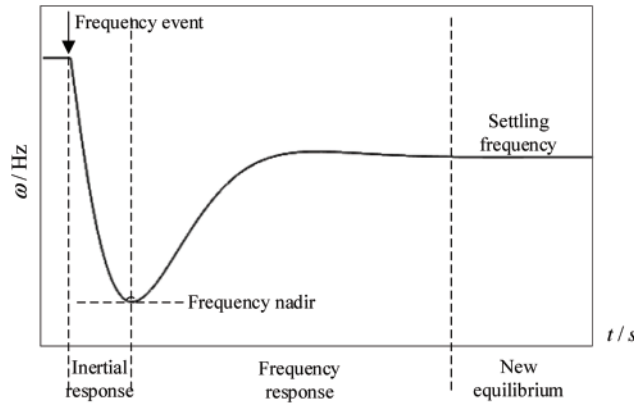
Figure 5: Inertial response and frequency modulation response of FVSG

3 The Relationship between the Frequency Characteristics of FVSG and *J*, *D*

3.1 Frequency Response of FVSG Input Power Disturbance

Considering only the influence of input power disturbance on frequency, without considering the impact of grid frequency variation, the equation can be obtained by making $\Delta\omega_g = 0$ in Fig. 4.

$$\frac{\Delta\omega}{\Delta P_{\text{in}}} = \frac{\dfrac{s}{J\omega_0}}{s^2 + \dfrac{D}{J}s + \dfrac{KD}{J(\omega_0 D + K)}}$$

The equation indicates that the system adjusts the FVSG power angle by adjusting the frequency ω, which is a second-order system. The change of the FVSG input power to the FVSG frequency is equivalent to a disturbance and then returns to the frequency before the trouble.

The oscillation angular frequency ω_n and damping ratio ζ of this transfer function are shown in the equation

$$\begin{cases} \omega_n = \sqrt{\dfrac{KD}{J(\omega_0 D + K)}} \\ \zeta = \dfrac{1}{2}\sqrt{\dfrac{D(\omega_0 D + K)}{JK}} \end{cases}$$

It can be seen from the equation that the larger the moment of inertia *J* is, the smaller the damping ratio and the smaller the oscillation angular frequency. The larger the damping coefficient *D*, the larger the damping ratio.

3.1.1 Overdamping

In the case of overdamping, let $p_{1,2} = \omega_n(\zeta \pm \sqrt{\zeta^2 - 1}), p_1 > p_2$, perform the inverse Laplace transform on the step response of the transfer function of equation and obtain equation

$$\Delta\omega = \Delta P_{\text{in}} \frac{e^{-p_2 t} - e^{-p_1 t}}{J\omega_0(p_1 - p_2)}$$

The maximum value of $\Delta\omega$ can be obtained by finding the extreme value of the derivative of the equation equal to 0. When the derivative is equal to 0, $t = \dfrac{\ln\dfrac{p_1}{p_2}}{p_1 - p_2}$ can be obtained, and the maximum value of $\Delta\omega$ can be obtained as shown in equation

$$\Delta\omega_{\max} = \frac{\Delta P_{\mathrm{in}}}{\sqrt{KJ\omega_0}} \left[\frac{\frac{1}{2}\sqrt{\dfrac{D(\omega_0 D + K)}{JK}} - \sqrt{\dfrac{D(\omega_0 D + K)}{4JK} - 1}}{\frac{1}{2}\sqrt{\dfrac{D(\omega_0 D + K)}{JK}} + \sqrt{\dfrac{D(\omega_0 D + K)}{4JK} - 1}} \right]^{\frac{1}{\sqrt{4 - \dfrac{D(\omega_0 D + K)}{4JK}}}}$$

3.1.2 Critical Damping

Similarly, when Critical damping, the maximum value of $\Delta\omega$ can be obtained as shown in equation

$$\Delta\omega_{\max} = \frac{\Delta P_{\mathrm{in}}}{\sqrt{J\omega_0 K}} e^{-1}$$

3.1.3 Underdamping

Similarly, when underdamped, the maximum value of $\Delta\omega$ can be obtained as shown in equation

$$\Delta\omega_{\max} = \frac{\Delta P_{\mathrm{in}}}{\sqrt{JK\omega_0}} e^{-\frac{\pi}{2} + \arcsin(\frac{1}{2}\sqrt{\frac{D(\omega_0 D + K)}{JK}})}$$

It can be seen from equations that the larger the moment of inertia J is, the smaller the frequency change of the VSG is, and the better the stability is.

3.2 Frequency Response When Grid Frequency Changes

Considering only the influence of grid frequency disturbance on FVSG frequency, without considering the influence of input power change, let $\Delta P_{\mathrm{in}} = 0$ in Fig. 4, we can get the equation

$$\frac{\Delta\omega}{\Delta\omega_{\mathrm{g}}} = \frac{\dfrac{KD}{J(\omega_0 D + K)}}{s^2 + \dfrac{D}{J}s + \dfrac{KD}{J(\omega_0 D + K)}}$$

The equation is a typical second-order system. The oscillation angular frequency ω_{n} and damping ratio ζ of this transfer function are shown in the equation below:

$$\begin{cases} \omega_{\mathrm{n}} = \sqrt{\dfrac{KD}{J(\omega_0 D + K)}} \\ \zeta = \dfrac{1}{2}\sqrt{\dfrac{D(\omega_0 D + K)}{JK}} \end{cases}$$

The adjustment time in the case of overdamping and critical damping is relatively long and is not considered.

When underdamped, the adjustment time t_s can be approximately expressed as an equation with an allowable error of 2%.

$$t_s \geq \frac{4}{\zeta \omega_n} = 8\frac{J}{D}$$

4 The Relationship between K, J of FVSG and the Capacity of Energy Storage Equipment and Its Charge-Discharge Characteristics

The energy storage device is directly related to the input power of the FVSG and the grid frequency disturbance, as well as the inertia coefficient and damping coefficient of the FVSG. The configuration of FVSG energy storage parameters is mainly to determine the inertia coefficient and damping coefficient according to the actual demand. The demand for energy storage is then determined based on the parameters of the FVSG, input power, and grid frequency disturbance. The following is mainly analyzed from two aspects of input power and grid frequency disturbance.

4.1 When the FVSG Input Power is Disturbed

When only analyzing the influence of input power disturbance on frequency, without considering the impact of grid frequency disturbance, let $\Delta\omega_g = 0$ in Fig. 4, we can get the equation

$$G_1(s) = \frac{\Delta P_{out}}{\Delta P_{in}} = \frac{\dfrac{KD}{J(\omega_0 D + K)}}{s^2 + \dfrac{D}{J}s + \dfrac{KD}{J(\omega_0 D + K)}}$$

The equation can be obtained from Fig. 1.

$$P_{in} = P_{out} + P_{es} = P_{in0} + \Delta P_{in} = P_{es} + P_{out0} + \Delta P_{out}$$

Thus, the charging and discharging power of the energy storage device can be obtained as in equation

$$P_{es} = \Delta P_{in} - \Delta P_{out}$$

The equation can be obtained from the work below:

$$P_{es} = \Delta P_{in} \frac{s^2 + \dfrac{D}{J}s}{s^2 + \dfrac{D}{J}s + \dfrac{KD}{J(\omega_0 D + K)}}$$

According to the physical meaning of inertia, the equation can be obtained

$$E_{es} = \frac{P_{es}}{s} = \Delta P_{in} \frac{s + \dfrac{D}{J}}{s^2 + \dfrac{D}{J}s + \dfrac{KD}{J(\omega_0 D + K)}}$$

Equation is the standard second-order transfer function model. The following analysis is divided into 3 cases according to different damping ratios, and the case of negative damping ($\zeta < 0$) is not considered because it is unstable.

4.1.1 Over-Damping

When the system is overdamped ($\zeta > 1$), the model shown in the equation has two different real roots. $p_{1,2} = \omega_n(\zeta \pm \sqrt{\zeta^2 - 1}), p_1 < p_2$.

The equation can be written as such

$$G_1(s) = \frac{\Delta P_{out}}{\Delta P_{in}} = \frac{1}{(T_1 s + 1)(T_2 s + 1)}$$

where, $T_1 = 1/p_1$, $T_2 = 1/p_2$.

The equation can be expressed as a cascade of two first-order systems when the damping coefficient is much larger than 1, when the pole p_2 is far from the imaginary axis and can be neglected. Therefore, the transfer function model shown in the equation above can be simplified to a first-order system as shown in equation below:

$$G_1(s) = \frac{\Delta P_{out}}{\Delta P_{in}} \approx \frac{1}{T_1 s + 1}$$

Generally, the step response reaches 95% to 98% of the steady-state value after aT_1 (where a takes the value of 3 to 4) time. Therefore, it can be considered that in the overdamped case, the regulation time of VSG, which is the response time required for energy storage, is shown in the equation below:

$$t_s \approx aT_1 = \frac{a\left(\zeta + \sqrt{\zeta^2 - 1}\right)}{\omega_n} \approx \frac{2a\zeta}{\omega_n}$$

When $t \rightarrow +\infty$, the maximum charge/discharge energy of the energy storage device can be obtained, and the total area of the shaded part shown in Fig. 6a is shown in the equation below:

$$E_{max} = \Delta P_{in}\frac{\omega_0 D + K}{K}$$

Therefore, it is known that when the input power is disturbed, the maximum charge and discharge energy of the energy storage device is also the minimum capacity of the energy storage device, and the minimum capacity of the required configuration of the energy storage capacity is shown in the equation.
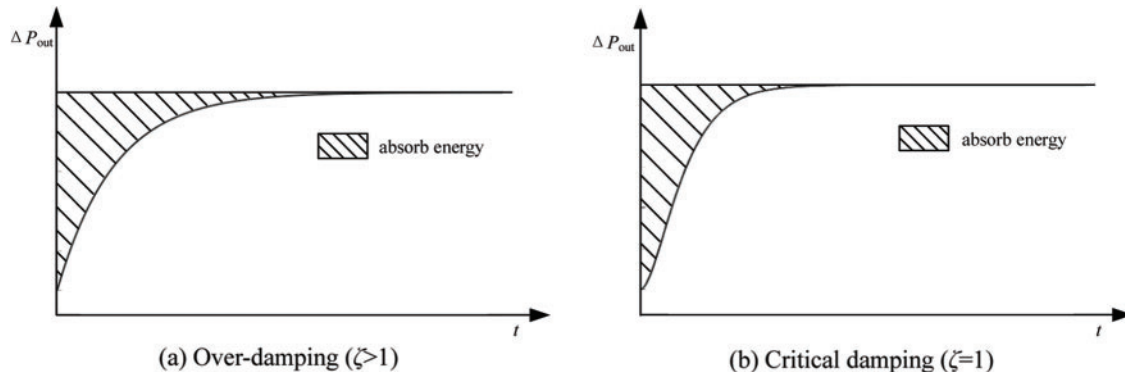

(a) Over-damping ($\zeta > 1$)   (b) Critical damping ($\zeta = 1$)

Figure 6: (Continued)

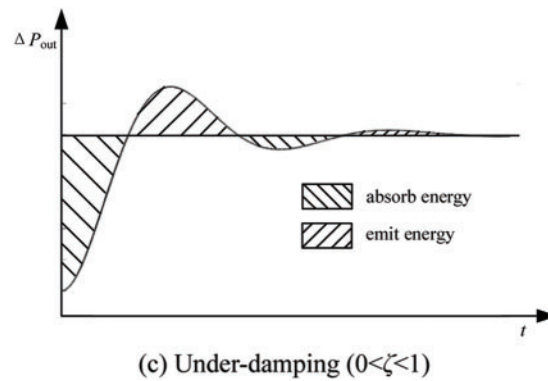(c) Under-damping ($0<\zeta<1$)

Figure 6: The step response process of FVSG with different damping

4.1.2 Critical Damping

When the system is critically damped ($\zeta = 1$), the transfer function shown in the equation has two identical real roots. $p_{1,2} = \omega_n$.

Thus, the mathematical model can be expressed as an equation

$$G_1(s) = \frac{\Delta P_{out}}{\Delta P_{in}} = \left(\frac{1}{Ts+1}\right)^2$$

where, $T_1 = 1/\omega_n$.

Similar to the case of over-damping, the regulation time of the system at this time $t_s = aT = a/\omega_n$.

When $t \to +\infty$, the maximum charge/discharge energy of the energy storage device can be obtained, and its mathematical model expression is consistent with overdamping. Therefore, it is known that when the input power is disturbed, the maximum charge/discharge energy of the energy storage device is also the minimum capacity of the energy storage device in the case of critical damping, and the minimum capacity of the required configuration of the energy storage capacity needs to satisfy the equation

$$E_{max} = \Delta P_{in} \left[\frac{\omega_0 D + K}{K} + \sqrt{\frac{J(\omega_0 D + K)}{KD}} e^{-\sqrt{\frac{D(\omega_0 D + K)}{4JK - D(\omega_0 D + K)}}\left(\pi - \arctan\sqrt{\frac{4JK - D(\omega_0 D + K)}{D(\omega_0 D + K)}}\right)} \right]$$

4.1.3 Underdamping

When the system is underdamped ($0<\zeta<1$), the equation has two characteristic roots with opposite numbers of each other. $p_{1,2} = -\omega_n(\zeta \pm j\sqrt{1-\zeta^2})$.

Let

$$\begin{cases} \omega_d = \sqrt{1-\zeta^2}\omega_n \\ \theta = a\tan\left(\frac{\sqrt{1-\zeta^2}}{\zeta}\right) \end{cases}$$

The time to reach the steady-state value for the first time is shown in the equation

$$t_r = \frac{\pi - \theta}{\omega_n \sqrt{1 - \zeta^2}} = \frac{\pi - \theta}{\omega_d}$$

The regulation time of the system is shown in the equation

$$\begin{cases} t_{s1} \approx \dfrac{3}{\zeta \omega_n} \\ t_{s2} \approx \dfrac{4}{\zeta \omega_n} \end{cases}$$

where, $0 < \zeta < 1$, t_{s1}, t_{s2} are the times of 95% and 98% overshoot, respectively, which are also the response times required by the energy storage device. The maximum charge/discharge energy of the energy storage device is obtained when the steady-state value is reached for the first time. The energy absorbed by the energy storage device throughout the step process, which is the area of the shaded part when the steady-state is reached as shown in Fig. 6c, is also the minimum capacity of the energy storage device and the minimum capacity of the required configuration of the energy storage capacity, as shown in equation

$$E_{max} = \Delta P_{in} \left[\frac{\omega_0 D + K}{K} + \sqrt{\frac{J(\omega_0 D + K)}{KD}} e^{-\sqrt{\frac{D(\omega_0 D + K)}{4JK - D(\omega_0 D + K)}} \left(\pi - \arctan \sqrt{\frac{4JK - D(\omega_0 D + K)}{D(\omega_0 D + K)}} \right)} \right]$$

In the case of over-damping, critical damping, and under-damping, the inertia coefficient J is less than, equal to, and greater than $\dfrac{D(\omega_0 D + K)}{4K}$, respectively. From the above analysis, it can be seen that the larger the damping coefficient is, the larger the capacity of the energy storage device is required. The over-damped case does not affect the charging and discharging the energy of the energy storage device. The larger the inertia coefficient in the case of under-damping, the larger the capacity of the energy storage device is needed.

4.2 FVSG Grid Frequency Disturbance

When only the influence of input power disturbance on frequency is analyzed, and the influence of grid frequency disturbance is not considered, let in Fig. 4, we can obtain equation

$$G_2(s) = \frac{\Delta P_{out}}{\Delta \omega_g} = -\frac{\dfrac{K\omega_0 D}{\omega_0 D + K} s + \dfrac{K\omega_0 D^2}{J(\omega_0 D + K)}}{s^2 + \dfrac{D}{J} s + \dfrac{KD}{J(\omega_0 D + K)}}$$

The equation can be obtained from the following:

$$\Delta P_{es} = \Delta \omega_g \frac{\dfrac{K\omega_0 D}{\omega_0 D + K} s + \dfrac{K\omega_0 D^2}{J(\omega_0 D + K)}}{s^2 + \dfrac{D}{J} s + \dfrac{KD}{J(\omega_0 D + K)}}$$

According to the physical meaning of inertia, equation can be obtained as the following:

$$E_{es} = \frac{P_{es}}{s} = \Delta\omega_g \frac{\frac{K\omega_0 D}{\omega_0 D + K}s + \frac{K\omega_0 D^2}{J(\omega_0 D + K)}}{s^3 + \frac{D}{J}s^2 + \frac{KD}{J(\omega_0 D + K)}s}$$

The charging and discharging of the energy from and of energy storage device consists of two main components: one is the difference between the output power of the FVSG and the input power after reaching the new steady-state due to the change in the frequency of the grid, and its charging and discharging power value is $-D\omega_0\Delta\omega_g$. By adjusting the input power P_{in} of the FVSG, so that $\Delta P_{in} = -D\omega_0\Delta\omega_g$ can offset this part of the charging and discharging demand.

If it cannot be regulated by the input power, this part of the energy storage capacity demand is $-D\omega_0\Delta\omega_g t_g$. The other part is the dynamic response process of the FVSG's inertia coefficient and damping coefficient directly related to the output power to grid frequency changes corresponding to the charging and discharging of energy storage devices. The following analysis is mainly for the second part of the charging and discharging of energy storage equipment.

The equation is the second-order transfer function model. The following analysis is performed in 3 cases according to different damping ratios, and the case of negative damping ($\zeta < 0$) is not considered because it is unstable.

4.2.1 Over-Damping

When the system is overdamped ($\zeta > 1$), the mathematical model shown in the equation has two different real roots. $p_{1,2} = \omega_n(\zeta \pm \sqrt{\zeta^2 - 1}), p_1 < p_2$.

When $t \to +\infty$, the maximum charging and discharging energy of the energy storage device, which is the total area of the shaded part shown in Fig. 6a, is obtained as shown in the equation

$$E_{max} = \Delta\omega_g \left[-\frac{D^2\omega_0^2 + D\omega_0 K}{K} + J\omega_0 \right]$$

Therefore it is known that when the grid frequency changes, the maximum charge and discharge energy of the energy storage device is also the minimum capacity of the energy storage device. The minimum capacity of the required configuration of the energy storage capacity needs to satisfy the equation.

4.2.2 Critical Damping

When the system is critically damped ($\zeta = 1$), the transfer function shown in the equation has two identical real roots. $p_{1,2} = \omega_n$.

When $t \to +\infty$, the maximum charge/discharge energy of the energy storage device can be obtained. Therefore, it is known that when the grid frequency changes, the maximum charge and discharge energy of the energy storage device is also the minimum capacity of the energy storage device, and the minimum capacity of the required configuration of the energy storage capacity is shown in the equation.

$$E_{\max} = -\Delta\omega_{\mathrm{g}}D\omega_0 \frac{4J\sqrt{JK}}{D\sqrt{D(\omega_0 D + K)}}$$

$$\left[\sqrt{\frac{D(\omega_0 D + K)}{JK}} - \sqrt{\frac{JK}{D(\omega_0 D + K)}} + \sqrt{\frac{JK}{D(\omega_0 D + K)}} \cdot \right.$$

$$\left. e^{-\sqrt{\frac{D(\omega_0 D + K)}{4JK - D(\omega_0 D + K)}} \left(\frac{\pi}{2} + \arctan \left[(1 - \frac{2JK}{D^2\omega_0}) \sqrt{\frac{D(\omega_0 D + K)}{4JK - D(\omega_0 D + K)}} \right] \right)} \right]$$

4.2.3 Underdamping

When the system is underdamped $(0 < \zeta < 1)$, the equation has two characteristic roots with opposite numbers of each other. $p_{1,2} = -\omega_{\mathrm{n}}(\zeta \pm j\sqrt{1 - \zeta^2})$.

When the steady-state value is reached, the maximum charge/discharge energy of the energy storage device is obtained. The energy absorbed by the energy storage device throughout the step process is the area of the shaded part in Fig. 6c when the steady-state is reached, which is also the minimum capacity of the energy storage device and the minimum capacity of the required configuration of the energy storage capacity, as shown in the equation

$$E_{\max} = -\Delta\omega_{\mathrm{g}}D\omega_0 \frac{4J\sqrt{JK}}{D\sqrt{D(\omega_0 D + K)}}$$

$$\left[\sqrt{\frac{D(\omega_0 D + K)}{JK}} - \sqrt{\frac{JK}{D(\omega_0 D + K)}} + \sqrt{\frac{JK}{D(\omega_0 D + K)}} \cdot \right.$$

$$\left. e^{-\sqrt{\frac{D(\omega_0 D + K)}{4JK - D(\omega_0 D + K)}} \left(\frac{\pi}{2} + \arctan \left[(1 - \frac{2JK}{D^2\omega_0}) \sqrt{\frac{D(\omega_0 D + K)}{4JK - D(\omega_0 D + K)}} \right] \right)} \right]$$

In the case of over-damping, critical damping and under-damping, the inertia coefficient J is less than, equal to and greater than $\dfrac{D(\omega_0 D + K)}{4K}$, respectively. From the above analysis, it can be seen that the larger the damping coefficient is, the larger the capacity requirement of the energy storage device is. The larger the inertia coefficient of the FVSG when overdamped, the smaller the capacity of the required energy storage device. When under damping, the larger the damping coefficient, the larger the capacity of the required energy storage equipment.

In summary, although different J and D parameters correspond to different ζ and different dynamic response characteristics, the minimum capacity required for the configuration of the energy storage unit in VSG has a consistent solution. The underdamped and critically damped cases have the same expressions for the energy storage capacity requirement, and the overdamped case is different. Table 1 shows the minimum capacity required to be configured for the energy storage unit.

Table 1: Capacity design of FVSG energy storage devices

Damping ratio	Minimum design capacity of energy storage equipment	
	Input power disturbance	Grid frequency change
Over-damping	Equation	Equation
Critical damping	Equation	Equation
Under-damping	Equation	Equation

5 Simulation Analysis

In order to verify the relationship between the charging and discharging power and capacity parameters of the energy storage device and the inertia coefficient and damping coefficient FVSG. Use Matlab/Simulink to build a simulation model. The relevant parameter settings are shown in Table 2.

Table 2: Parameters of FVSG

Parameter	Unit	Value		
		Overdamped ($\zeta = 10$)	Critical damping ($\zeta = 1$)	Underdamped ($\zeta = 0.707$)
J	kg·m^2	268	268	546
D	N·m·s	84682	1068	1068
K	W·rad^{-1}		1×10^7	
ω_0	rad·s^{-1}		10π	
U_0	kV		6.6	

In the simulation of charging and discharging energy, when the FVSG input power is disturbed, ΔP_{in} selects 1 MW. In the simulation of charging and discharging energy when the grid frequency is disturbed, $\Delta \omega_g$ select 6.28 rad/s.

5.1 FVSG Robustness Optimization Verification

The under-damped parameters in Table 2 are selected to verify the robustness of the FVSG. The results are shown in Fig. 7.

It can be seen from the Fig. 7 that the output power of the VSG with the feedforward branch changes smoothly when the system is disturbed by the input power or when the grid frequency changes, and eventually stabilizes gradually. In contrast, the output power of the VSG without feedforward branching changes dramatically when the system is subjected to input power disturbance or grid frequency change, and then stabilizes after a period of time. Therefore, the VSG with feedforward branching facilitates the stable output power change.
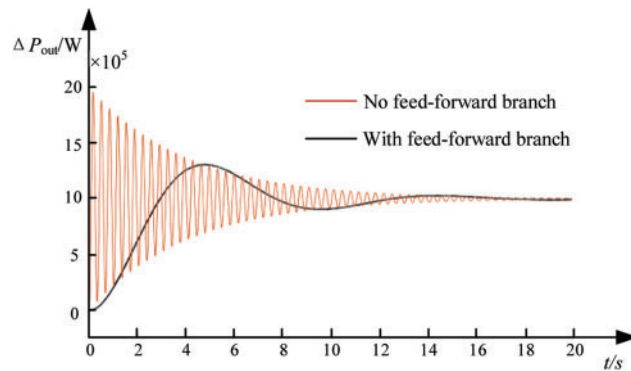
Figure 7: Comparison of output power with and without the feedforward branch during perturbation

5.2 Verification of the Relationship between FVSG Parameters and Frequency Characteristics

The simulation curve of the frequency response when the input power is disturbed is shown in Fig. 8.
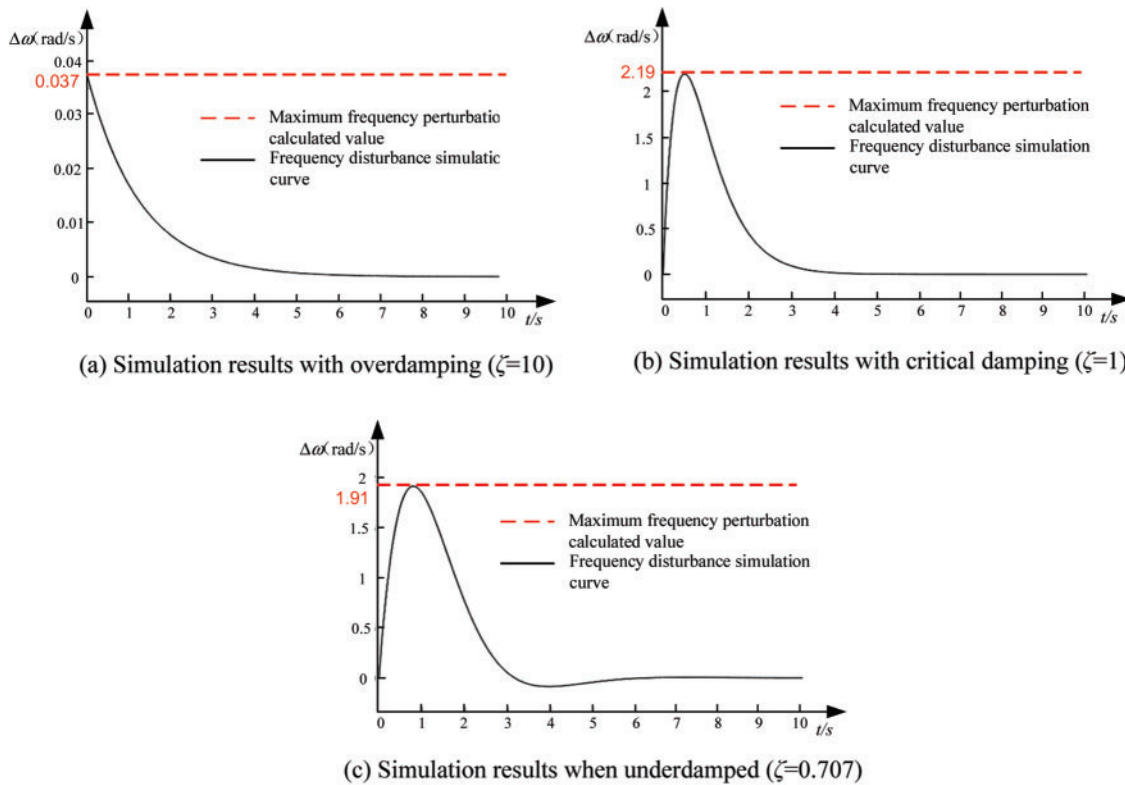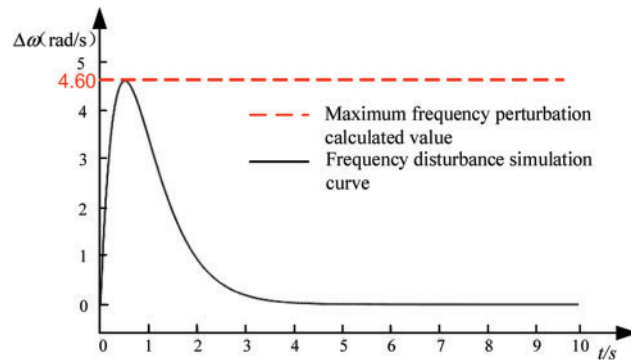

Figure 8: Simulation diagram of frequency characteristics of FVSG when input power is perturbed

The simulation results in Fig. 8 verify the equation.

When the grid frequency is disturbed, the critical damping parameters in Table 2 are used, and the frequency response time simulation curve FVSG is shown in Fig. 9.

Figure 9: Simulation diagram of frequency characteristics of FVSG when grid frequency is disturbed

The simulation results in Fig. 9 verify the equation.

5.3 Verification of the Relationship between FVSG Parameters and the Capacity of Energy Storage Equipment

The parameters of Table 2 are selected for the design and the results are shown in Fig. 10 by simulating the E_{max} equation.
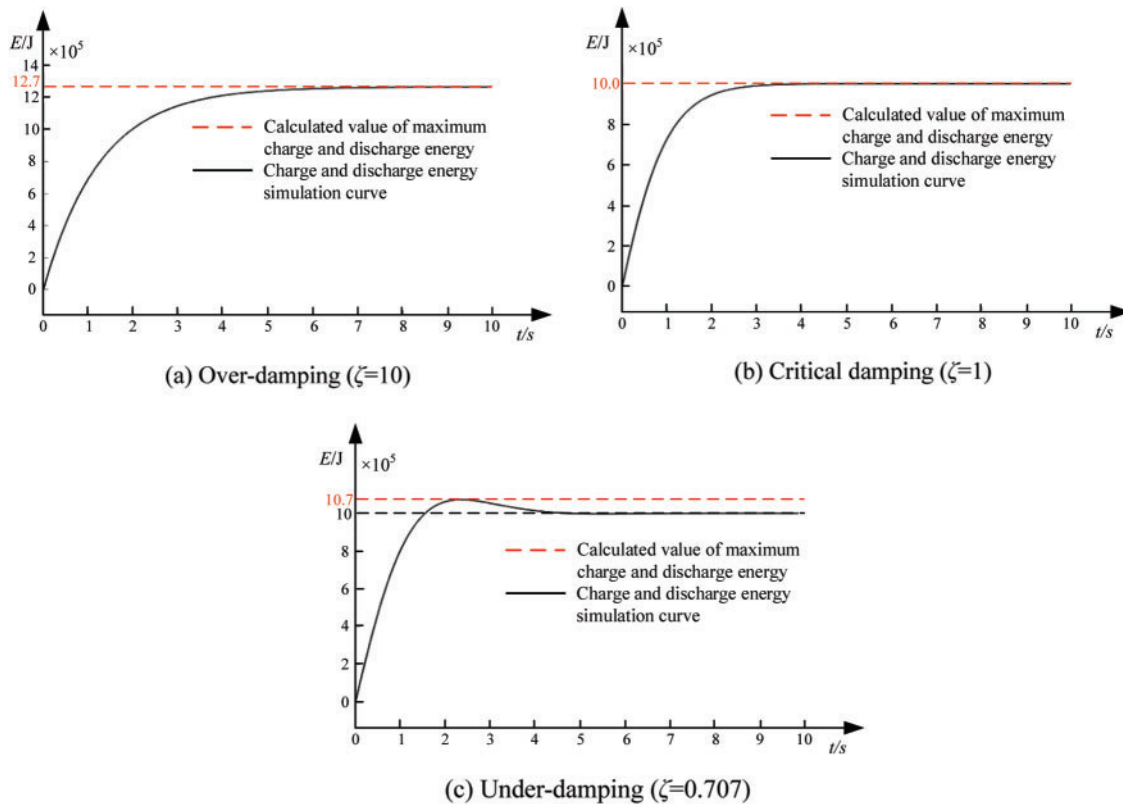

(a) Over-damping (ζ=10)

(b) Critical damping (ζ=1)

(c) Under-damping (ζ=0.707)

Figure 10: Simulation diagram of FVSG parameters and capacity of energy storage equipment

The simulation results in Fig. 10 verify the equation, respectively.

The minimum energy storage device design should meet the maximum value of charging and discharging energy to ensure the maximum charging and discharging demand required when output power disturbances or grid frequency changes occur.

The parameters of Table 2 under-damping are selected, and the inertia coefficient J and damping coefficient D are changed respectively to simulate the output power, and the results are shown in Fig. 11.
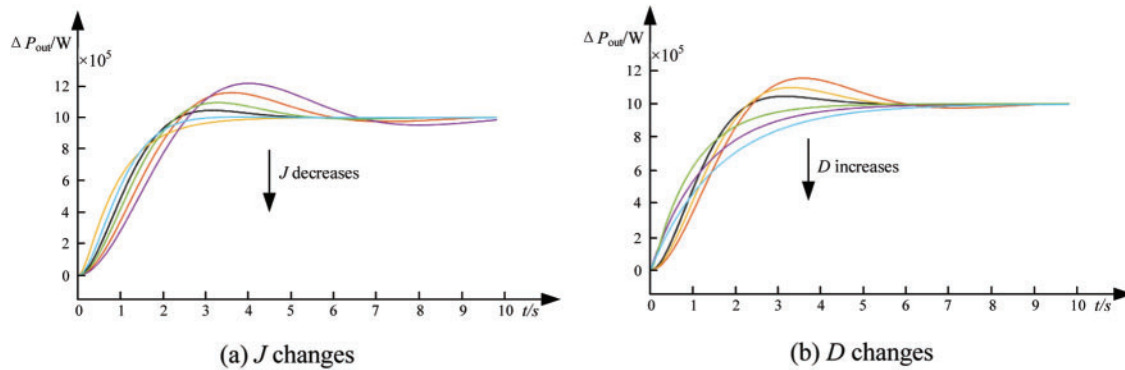

Figure 11: Effect of FVSG parameters on output power

It can be seen from Fig. 11 that the smaller the inertia coefficient J of FVSG, the shorter the output power adjustment time and the smaller the output power variation rate. the larger the damping coefficient D of FVSG, the shorter the output power adjustment time and the smaller the output power variation rate, the smaller the oscillation amplitude, and the better the anti-interference performance of FVSG.

As can be seen from Fig. 11, when the input power is disturbed, the output power increases, then the energy storage unit is required to absorb the power and maintain the stability of the output power. From the perspective of the second-order output power response performance of the VSG, when the damping factor is equal to 0.707, the rate of change of the output power of the VSG is small and the adjustment time is small.

In the actual selection of parameters, it is also necessary to combine with the actual situation, a comprehensive cost-effective consideration, and the selection of appropriate parameters together.

6 Conclusion

In this paper, the relationship among frequency characteristics, inertia coefficient, damping coefficient, and energy storage capacity of FVSG is deduced in detail. Matlab/Simulink carries out the simulation verification. Research indicates:

(1) FVSG robustness is optimised to maintain its relative stability during input power perturbations and grid frequency changes, improving the adaptiveness of the parameters.

(2) Changing the inertia and damping coefficients has a greater impact on the fluctuation of the output power. The smaller the inertia coefficient and the larger the damping coefficient, the better the stability of the output power. Combined with economic considerations, the FVSG has better immunity to interference at a damping factor of 0.707.

(3) In order to improve the immunity of the FVSG, the inertia and damping coefficients need to be increased, as well as a larger capacity of the energy storage device. When the energy

storage capacity of the FVSG is insufficient, the output of the FVSG will not be controlled as expected and will cause voltage fluctuations. Therefore, the actual design has to meet the minimum charge and discharge requirements of the FVSG.

Conflicts of Interest: The authors declare that they have no conflicts of interest to report regarding the present study.

References

1. Yan, X. W., Zhang, W. C. (2019). Review of VSG control-enabled universal compatibility architecture for future power systems with high-penetration renewable generation. *Applied Sciences, 9(7),* 1484. DOI 10.3390/app9071484.

2. Lopes, J. A. P., Hatziargyriou, N., Mutale, J. (2007). Integrating distributed generation into electric power systems: A review of drivers, challenges and opportunities. *Electric Power Systems Research, 77(9),* 1189–1203. DOI 10.1016/j.epsr.2006.08.016.

3. Yan, X. W., Xu, Y. (2019). Multiple time and space scale reactive power optimization for distribution network with multi-heterogeneous RDG participating in regulation and considering network dynamic reconfiguration. *Transactions of China Electrotechnical Society, 34(20),* 4358–4372. DOI 10.19595/j.cnki.1000-6753.tces.181933.

4. Zhang, W. C., Liang, H. F., Bin, Z. (2012). Review of DC technology in future smart distribution grid. *IEEE PES Innovative Smart Grid Technologies*, pp. 1–4. Tianjin, China.

5. Guarnieri, M. (2015). More light on information. *IEEE Industrial Electronics Magazine, 9(4),* 58–61. DOI 10.1109/MIE.2015.2485182.

6. Zhang, C. Y., Dou, X. B., Sheng, W. X. (2020). A robust virtual synchronization control strategy for distri-buted photovoltaic clusters. *Proceedings of the CSEE, 40(2),* 510–521. DOI 10.13334/j.0258-8013.pcsee.182424.

7. Albu, M., Visscher, K., Creanga, D. (2009). Storage selection for DG applications containing virtual synchronous generators. *IEEE Bucharest PowerTech*, pp. 1–6. Bucharest, Romania.

8. Falahi, G., Huang, A. (2014). Low voltage ride through control of modular multilevel converter based HVDC systems. *40th Annual Conference of the IEEE Industrial Electronics Society*, pp. 4663–4668. Dallas, TX, USA.

9. Cheng, M., Zhu, Y. (2014). The state of the art of wind energy conversion systems and technologies: A review. *Energy Conversion and Management, 88,* 332–347. DOI 10.1016/j.enconman.2014.08.037.

10. Zhong, Q. C. (2017). Power-electronics-enabled autonomous power systems: Architecture and technical routes. *IEEE Transactions on Industrial Electronics, 64(7),* 5907–5918. DOI 10.1109/TIE.2017.2677339.

11. Geng, H., Yang, G. (2018). Modeling framework of voltage-source converters based on equivale-ence with synchronous generator. *Modern Power Systems, 6(6),* 1291–1305. DOI 10.1007/s40565-018-0433-1.

12. Zhang, B. Q., Hu, C. B., Ma, L. F. (2019). Active power quality control for microgrid with virtual synchronous generator based on small-signal stability analysis. *Automation of Electric Power Systems, 43(23),* 210–222.

13. Chen, J. K., Zeng, Q., Xin, Y. C. (2020). Secondary frequency regulation control strategy of MMC-MTDC converter based on improved VSG. *Power System Technology, 44(4),* 1428–1436. DOI 10.13335/j.1000-3673.pst.2019.1227.

14. Daili, Y., Harrag, A. (2019). New model of multi-parallel distributed generator units based on virtual synchronous generator control strategy. *Energy, Ecology and Environment, 4(5),* 222–232. DOI 10.1007/s40974-019-00128-3.

15. Yan, X. W., Cui, S., Chang, W. (2021). Primary frequency regulation control strategy of doubly-fed induction generator considering supercapacitor SOC feedback adaptive adjustment. *Transactions of China Electrotechnical Society, 36(5),* 1027–1039.

16. Yan, X. W., Lü, J. W., Jia, J. X. (2020). Two-stage active standby photovoltaic virtual synchronous machine control strategy. *Power System Protection and Control, 48(15),* 61–68.

17. Gao, J. R., Li, G. J., Wang, K. Y., Wu, P., Yu, Z. M. (2020). Control of grid-connected PV-battery virtual synchronous machine considering battery charging/discharging power limit. *Automation of Electric Power Systems, 44(4),* 134–141.

18. Lu, F. Z., He, A. R., Hou, K. (2019). Low-voltage ride-through control strategy of virtual synchronous generator based on the all-pass filter. *Electric Power Automation Equipment, 39(5),* 176–181. DOI 10.16081/j.issn.1006-6047.2019.05.026.

19. Alipoor, J., Miura, Y., Ise, T. (2015). Power system stabilization using virtual synchronous generator with alternating moment of inertia. *IEEE Journal of Emerging and Selected Topics in Power Electronics, 3(2),* 451–458. DOI 10.1109/JESTPE.2014.2362530.

20. Li, D., Zhu, Q., Lin, S. (2017). A self-adaptive inertia and damping combination control of VSG to support frequency stability. *IEEE Transactions on Energy Conversion, 32(1),* 397–398. DOI 10.1109/TEC.2016.2623982.

21. Li, X., Chen, G., Ali, M. S. (2019). Improved virtual synchronous generator with transient damping link and its seamless transfer control for cascaded H-bridge multilevel converter-based energy storage system. *IET Electric Power Applications, 13(10),* 1535–1543. DOI 10.1049/iet-epa.2018.5722.

22. Hong, H. H., Gu, W., Huang, Q. (2019). Power oscillation damping control for microgrid with multiple VSG units. *Proceedings of the CSEE, 39(21),* 6247–6254. DOI 10.13334/j.0258-8013.pcsee.181088.

23. Zeng, Z., Shao, W. H., Ran, L. (2015). Mathematical model and strategic energy storage selection of virtual synchronous generators. *Automation of Electric Power Systems, 39(13),* 22–31. DOI 10.7500/AEPS20140901007.

24. Song, Q., Zhang, H., Sun, K. (2017). Improved adaptive control of inertia for virtual synchronous generators in islanding micro-grid with multiple distributed generation units. *Proceedings of the CSEE, 37(2),* 412–423. DOI 10.13334/j.0258-8013.pcsee.161658.

25. Shi, R., Zhang, X., Hu, C. (2018). Self-tuning virtual synchronous generator control for improving frequency stability in autonomous photovoltaic-diesel micro grids. *Journal of Modern Power Systems and Clean Energy, 6(3),* 482–494. DOI 10.1007/s40565-017-0347-3.

26. Yang, F., Shao, Y. L., Li, D. D. (2020). A fuzzy adaptive VSG control strategy considering energy storage capacity and constraint of SOC. *Power System Technology, 1,* 1–12.

27. Xing, D. F., Tian, M. X. (2021). Relationship between frequency characteristics of virtual synchronous generator and parameters of energy storage equipment. *Power System Technology, 45(9),* 3582–3593. DOI 10.13335/j.1000-3673.pst.2020.1490.

28. Meng, J. H., Zhao, P. H., Wang, Y. (2020). Research on the cooperative operation of optical storage system based on virtual inertial control. *Power System Technology, 4,* 1–12.

29. Chen, J., O'Donnell, T. (2019). Parameter constraints for virtual synchronous generator considering stability. *IEEE Transactions on Power Systems, 34(3),* 2479–2481. DOI 10.1109/TPWRS.59.

30. Chen, J., O'Donnell, T. (2019). Analysis of virtual synchronous generator control and its response based on transfer functions. *IET Power Electronics, 12(11),* 2965–2977. DOI 10.1049/iet-pel.2018.5711.